JOURNAL OF AIRCRAFT
Vol. 45, No. 6, November–December 2008

Design Forum

DESIGN FORUM papers range from design case studies to presentations of new methodologies to speculations about emerging design trends. They vary from 2500 to 12,000 words (where a figure or table counts as 200 words). Following informal review by the Editors, they may be published within a few months of the date of receipt. Style requirements are the same as for regular contributions (see inside back cover).

Development of a Four-Rotor Cyclocopter

In Seong Hwang,* Seung Yong Min,* Choong Hee Lee,* and Seung Jo Kim†
Seoul National University, Seoul 151-742, Republic of Korea

DOI: 10.2514/1.35575

A cyclocopter propelled by a cycloidal blade system is a new concept of vertical takeoff and landing aircraft. The cycloidal blade system, which can be described as a horizontal rotary wing, offers powerful thrust levels and a unique ability to change the direction of the thrust almost instantly. This paper investigates the development of the cyclocopter with four rotors. The aircraft was designed through computational fluid dynamics and finite element structural analyses. Elliptic blades and a swash plate were applied to the rotor system to improve the rotor performance and control mechanism. Efficient dc brushless motors and lithium-polymer batteries were used for power transmissions. Almost all parts of the rotor blades and fuselage were manufactured out of composite material. Thrust and required power were measured experimentally on the test bed. The experimental result shows that the cyclocopter can produce sufficient thrust for both hovering and low-speed forward flight.

Nomenclature

c	=	blade chord length
E	=	modulus of elasticity
f_c	=	natural frequency due to concentrated mass
f_d	=	natural frequency due to distributed mass
g	=	acceleration of gravity
I	=	area moment of inertia
I_b	=	mass moment of inertia
L	=	shaft length
M	=	concentrated mass
T	=	torque
w	=	distributed mass
ε	=	tilt angle of thrust direction
θ	=	pitch angle
$\theta_{\max}$	=	maximum pitch angle
φ	=	azimuth angle
ω	=	rotor rotating speed

I. Introduction

A CYCLOCOPTER is a rotary-wing aircraft that produces thrust by a cycloidal blade system [1]. The rotor system consists of several blades rotating about a horizontal axis, which is perpendicular to the direction of normal flight. The rotor blades of the cyclocopter experience a periodic pitch angle variation during rotor rotation. This feature provides the rotor the capabilities to change the direction and the magnitude of thrust instantly and easily. This characteristic gives the aircraft good maneuverability including vertical takeoff and landing (VTOL), hovering, and low-speed forward flight. Unlike a conventional helicopter rotor, the cycloidal rotor blades operate at a constant speed along the entire blade span, allowing all the blade elements to operate at their peak efficiency and causing the inflow in the spanwise direction to be uniform. Moreover, the cycloidal rotors operate at a much lower rotational speed than conventional helicopter rotors, leading to a very low noise level. This is an essential advantage in various missions, such as close observation, flying in an urban environment, and military purposes. However, the cycloidal rotor also has several drawbacks caused by its relatively big rotating structure. A conventional helicopter rotor creates a 2-D disk, whereas the cycloidal rotor creates a 3-D cylinder. This gives a weight penalty to the cyclocopter when compared with a conventional helicopter rotor.

The cycloidal rotor system was studied at several institutes, including NACA and the University of Washington from the 1920s to 1940s [2–7]. Researchers tested cycloidal rotors in a wind tunnel or they built ground test models to investigate their possibilities as an aircraft. Although the performance was good in theory and experimental results supported the theoretical values, all designs failed to be successful in flight. In the late 1990s, when almost 50 years had passed since World War II, the research into the cycloidal mechanism was resumed at Bosch Aerospace [8,9]. In the ground test of the six-bladed cycloidal rotor, they obtained a high thrust per unit power. The cycloidal blade system was also applied to airship control and a ducted fan, in addition to an aircraft by this company. Recently, several other researchers began developing the cycloidal rotor for an aircraft propulsion system [10–13].

This paper describes the development of the cyclocopter. The designs of the rotor, control mechanism, and power transmission were investigated along with the experiments necessary to verify the performance as an aircraft. Although many parametric studies and optimizations were carried out in design stages, this paper only describes the summarized results. In the rotor design step, the

Presented as Paper 2247 at the 48th AIAA/ASME/ASCE/AHS/ASC Structures, Structural Dynamics, and Materials Conference, Honolulu, HI, 23–26 April 2007; received 12 November 2007; revision received 6 May 2008; accepted for publication 17 May 2008.

*Graduate Student, School of Mechanical and Aerospace Engineering.
†Professor, School of Mechanical and Aerospace Engineering; Director, Flight Vehicle Research Center. Associate Fellow AIAA

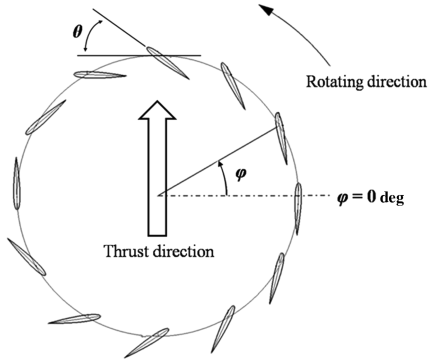

Fig. 1 Concept of the cycloidal blade system.

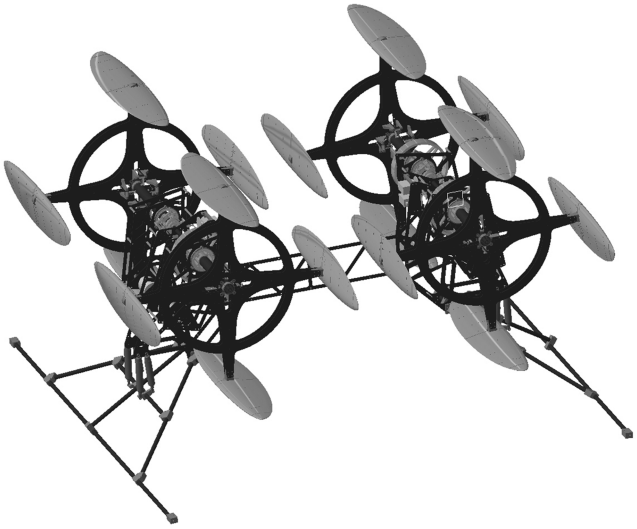

Fig. 2 Designed cyclocopter.

characteristics of the cycloidal rotor itself were referred by Yun [1], and the rotor blade configuration was determined through a computational fluid dynamics (CFD) analysis. A structurally safe blade was also designed through finite element analysis. The swash plate was adopted during the control system design to improve the control performance. High performance brushless motors and lithium-polymer (Li-Po) batteries were selected as the power resources. Among the design steps performed, the details of the design were omitted from this paper and the accuracy of the analysis in [1] was accepted. Figure 1 shows the concept of the cycloidal blade system. In this figure, the blade pitch angle θ is maximized at the positions of the azimuth angle φ 90 and 270 deg, producing a thrust in an upward direction. Figure 2 shows the entire designed cyclocopter. The aircraft consists of four rotors. Two pairs of rotors rotate in opposite directions to compensate for the resulting antitorque. Each rotor has four elliptic blades and the blade is supported at the center position that is connected with the hub arm. The rotors are operated by their own motor systems and control devices, allowing for control of the pitch angle and rotating speed independently.

II. Design of Rotor System

Although the cyclocopter is propelled by a rotating blade system, the characteristics of the cyclocopter blade are close to those of a fixed wing aircraft, because the blades and the rotor shaft are parallel to each other. The designed cyclocopter in Fig. 2 has 16 blades, and so it is important to reduce the drag of each blade. Therefore, the elliptic shape blade was adopted based on Prandtl's classical lifting line theory, to minimize the induced drag and to reduce the required power of the cyclocopter rotor system [14]. Furthermore, the elliptic shape blade is more appropriate than the rectangular shape blade because it reduces the blade bending moment with a single point supporting structure.

A. Computational Fluid Dynamics Analysis

The aerodynamic design variables of the cyclocopter rotor are not limited on the number of blades, airfoil, rotor radius, rotating speed, maximum pitch angle, span, and chord length of the blade. Among these variables, the number of blades is fixed at four and the airfoil is determined to be a NACA0018 in this paper, because these design values are efficient in this system according to previously conducted research [1,15]. Other variables influence each other, for example, the rotor efficiency becomes better when the rotor radius is larger, even though a large radius causes structural weakness when the blade tip speed is constant [1]. Therefore, the cyclocopter rotor system should be designed optimally by considering the related variables simultaneously.

A 2-D CFD parametric study was carried out for rotor optimization. A CFD mesh was generated automatically by the PCL (Patran Command Language) of MSC.PATRAN [16] and the commercial CFD software, STAR-CD was used for the CFD analysis [17]. In particular, the moving mesh method was adopted to simulate rotor blades, which have a periodic pitch angle variation. Figure 3 shows some of the results, including thrust and power variation according to the chord length. The graphs show a thrust of 136 N at 1940 W when the chord length is 0.08 m and the pitch angle is 28 deg at a rotating speed of 1200 rpm, a blade span length of 0.5 m, and a rotor radius of 0.25 m. The other relationships obtained from the calculation are as follows: thrust is proportional to the quadratic order of the rotating speed increase, the required power is proportional to the cubic order of the rotating speed increase, the pitch angle variation is almost linearly related to thrust and the required power at the calculated range (between 20 and 30 deg), the thrust per unit power increases approximately 20% when the blade

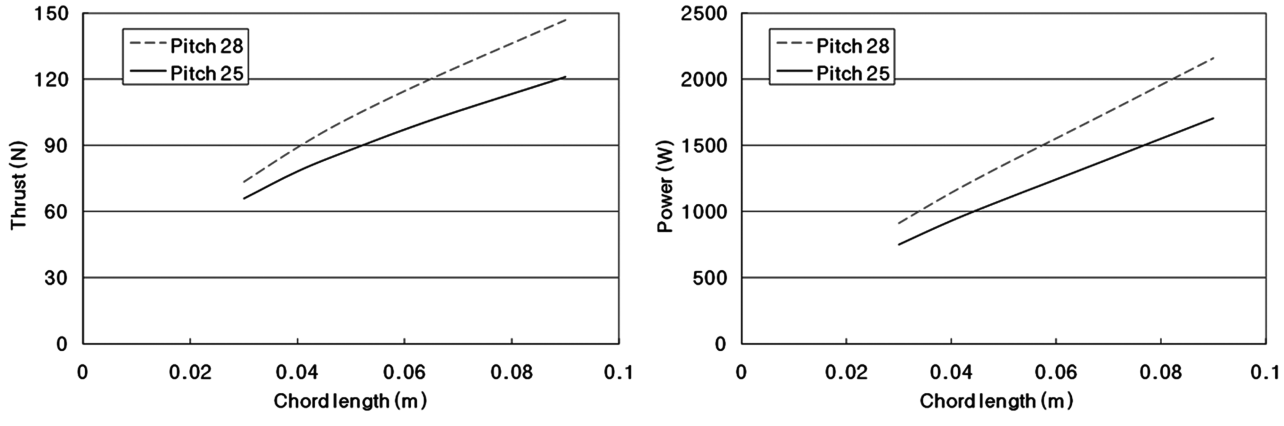

Fig. 3 Thrust and power variations from the 2-D CFD analysis.

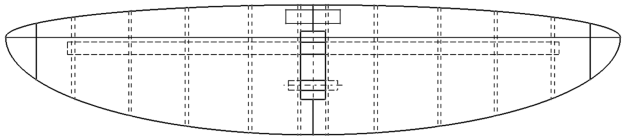

Fig. 4 Planform of the elliptical blade.

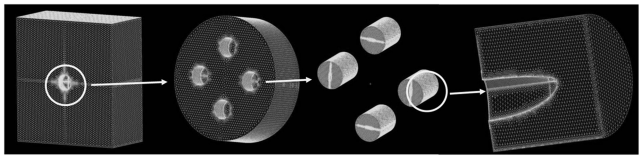

Fig. 5 Mesh generation for the 3-D CFD analysis.

pivot point moves from 0.5 to 0.25c, and the flow tilt angle changes from 15 to 45 deg because of the flow interference among the rotors.

The geometric shape of the blade is determined based on the results of the 2-D analysis, and Fig. 4 shows the resulting planform of the blade. The length of the major axis is a blade span length of 0.5 m, and the ratio of the minor axes is 1:3 to coincide with the 25% point of chord, which is the aerodynamic center of the NACA0018. The longest chord length is 0.105 m at the central position. The surface area of this elliptical blade is almost the same as that of a rectangular blade of chord length 0.08 m, as shown in Fig. 3. According to the CFD results, centrifugal force, and blade manufacturing, the blade pivot point was found to be 0.33c. According to the CFD calculation with a pivot point variation, the thrust was maximized when the pivot point was around 0.3c. The pivot point should be coincident with the c.g. point of the blade to reduce the centrifugal force acting on the control rod.

A 3-D CFD analysis was carried out for the detail analysis based on the preceding results. The moving mesh method was applied, which is the same as in the 2-D analysis. Parallel computing was used by partitioning the domains into several regions: the blade region doing periodic motion, the rotor region doing rotation, and the exterior region. One side of the blade was modeled by using the symmetric boundary condition, as shown in Fig. 5. Table 1 shows analysis conditions for this simulation. There are approximately 3.7 million total cells with a four-node tetrahedron element. Eight CPUs were used for this parallel computing. The rotating speed and maximum pitch angle are variables in this analysis. Figure 6 shows the thrust and power variations according to the rotating speed at a maximum pitch angle of 28 deg. Figure 7 shows the thrust variation according to the maximum pitch angle at a rotating speed of 1130 rpm. As shown in Figs. 6 and 7, the 3-D results are slightly higher than the 2-D results, and the 3-D results for four rotors are closer to the experimental values than the 2-D results, which will be shown later in this paper.

Table 1 Analysis condition

Analysis type	3-D transient
Mesh type	Unstructured (tetra)
Total number of cells	3,681,648
Moving mesh type	Arbitrary siding interface
Turbulence model	k-ε/high Reynolds
Number of steps	1000
Parallel computing	8 CPUs
Variables	rpm and pitch angle

Table 2 shows the designed parameters obtained from the CFD analysis. When the rotor rotates at 1130 rpm, the cyclocopter produces a thrust of 166 N at 2240 W. These values are acceptable because the estimated weight of designed cyclocopter is approximately 10 kg and selected power sources (dc electric motors) produce 2240 W after considering the motor efficiency and mechanical loss of the rotor system.

B. Structural Analysis

Figure 8 shows the section view of the blade at the central position in the span direction. The spar is located at the 33% position from the leading edge, and the control linkage is connected at the 62% position. The center of gravity is coincident with the spar. Figure 9 shows the assembled picture of the rotor blade. The circular spar made of a carbon composite material is the main structure of the loading support, and the blade shape is formed by the skin and rib. The blade is connected to the hub arm at the pivot point through two ball bearings. The center rib is reinforced by a woven glass composite to ensure the blade can endure the highest stress value.

A structural analysis was carried out for the designed cyclocopter rotor system. The cyclocopter rotor blades are loaded by both aerodynamic and centrifugal forces during its rotation, and the centrifugal force is relatively high compared with the aerodynamic force. The forces acting on the blades cause a bending moment, which causes the blades to deform. A stress concentration could occur at the central position of the blade, which is connected to the hub arm. The blade deformation causes the aerodynamic performance to be low and the stress concentration causes the blade's destruction. Therefore, it is important to design the blade with a high enough strength and a light weight. The blade was designed and manufactured out of a composite material, which has a good strength-to-weight ratio. MSC.NASTRAN was used for the structural analysis of the designed rotor blade system [18].

Figure 10 shows the finite element model of the rotor blades. The mesh was generated by MSC.PATRAN. The spar and control linkage were modeled with 1-D beam (bar2) elements, whereas the other parts were modeled with 2-D shell (quad4) elements. A boundary condition of the free pitching motion was applied to the hub arm, spar, and control parts using multipoint constraints.

A static analysis was carried out for the cyclocopter rotor blades rotating at 1200 rpm by the nonlinear static solution method (sol 106)

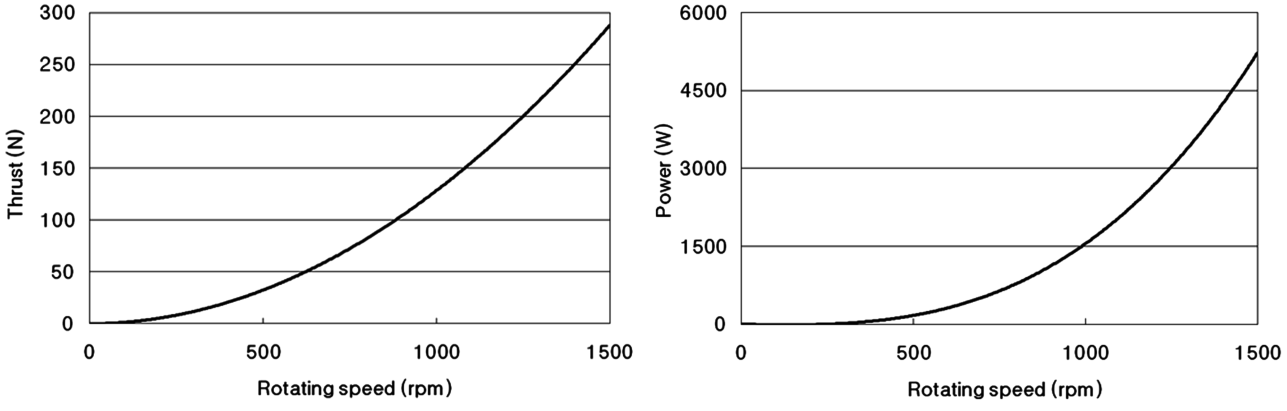

Fig. 6 Thrust and power variations according to the rotating speed.

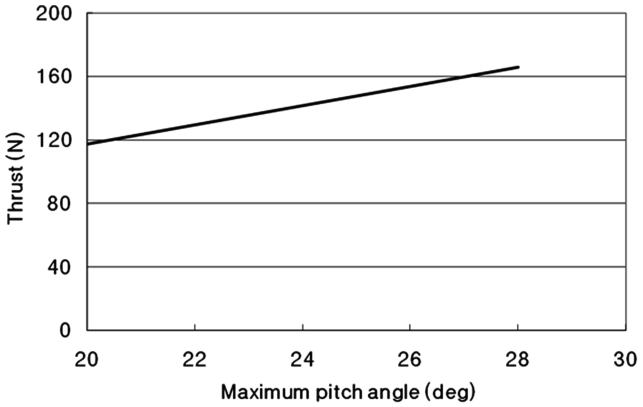

Fig. 7 Thrust variation according to the maximum pitch angle.

of MSC.NASTRAN. Figure 11 shows the analytic results of the displacement. The maximum displacement value is 3.26 mm at the blade tip, whereas the circular carbon spar is deformed by 1.48 mm at the same analysis condition. The maximum stress of 115 MPa occurs at the middle position of the spar, which is connected to the hub arm. At the same condition, the maximum stress on the blade skin is 34.5 MPa. These values are within the statically safe criteria; therefore, these design variables are acceptable.

The cyclocopter rotor blade system vibrates during rotation. Dynamic instability, which could occur due to this vibration, should be avoided by taking into consideration resonance, which is defined as the coincidence between the natural frequency and the forcing frequency. Therefore, a dynamic analysis of the rotor was carried out. Figure 12 shows the mode shapes. The first shape occurs due to the twist motion between the rigid blade and the rigid hub arm. The lowest four mode shapes are similar to this motion and, in particular, the second and third eigenvalues are the same figure. These mode shapes are caused by the one-point joint structure that connects the stiff blade with the stiff hub arm. The corresponding frequencies are 36.1, 39.0, and 41.2 Hz. The next four modes occur due to the deformation of the hub arm, as shown in Fig. 12. The mode frequency of the blade deformation is relatively high, therefore the vibration of the blade itself does not affect the dynamic instability.

III. Design of the Control System

The appropriate control mechanism is required to allow the cyclocopter to maneuver during hovering and forward flight. The control system is quite different from that of a conventional rotorcraft. A new mechanical and dynamic control system should be designed to satisfy the minimum control force, be of light weight, be rapid, and provide accurate servo control. This research applies the swash plate to the cyclocopter rotor control mechanism for performance improvement.

The purpose of using the swash plate is to decrease the whirling of the cantilever shaft by enlarging the shaft diameter, to make the control devices compact, and to be located inside the fuselage. The control mechanism of the cyclocopter in previous research changes the pitch angle and phase angle to control the thrust direction and magnitude [1]. However, the rotor control system developed in this research only changes the pitch angles in the back/forth and up/down directions. This new mechanism enables easier yawing control of the aircraft, in addition to the performance improvement of converting the flying mode from hovering to forward flight. Furthermore, this control mechanism shows a faster response than the previous control design.

Table 2 Designed parameters of the cyclocopter rotor system

Number of rotors	4
Number of blades (for one rotor)	4
Airfoil	NACA0018
Rotor radius	0.25 m
Blade span length	0.5 m
Blade chord length (largest value)	0.105 m
Thrust	166 N
Required power	2240 W

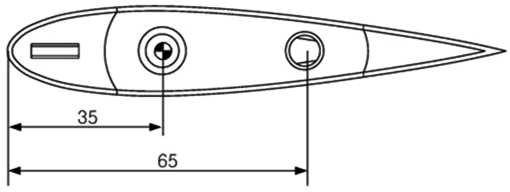

Fig. 8 Section view of the blade.

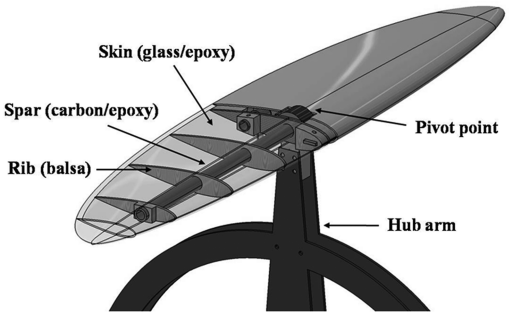

Fig. 9 Assembled picture of the rotor blade.

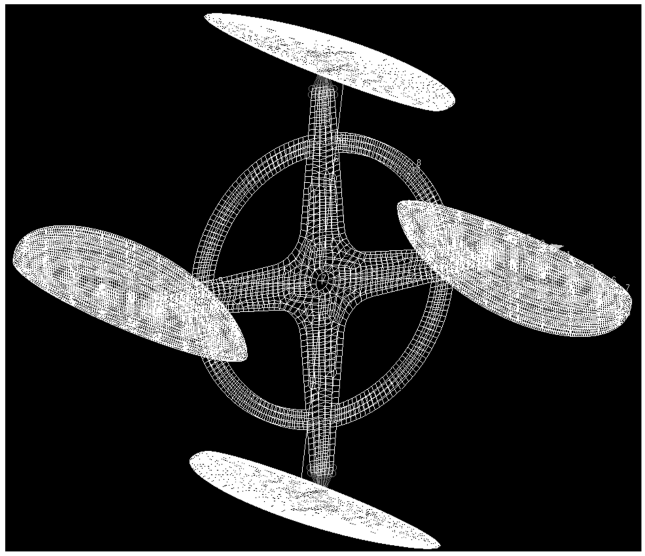

Fig. 10 Finite element mesh of the cyclocopter rotor.

The control force acted on the control linkage by the blade inertia was calculated. The mass moment of inertia at the blade pivot point is 5.002e-6 kgm^2 when the rotor rotating speed is 1200 rpm and the maximum pitch angle is 30 deg. The pitch angle is represented as Eq. (1), where ε is the tilt angle of the thrust direction:

$$\theta = \theta_{\max} \sin(\varphi + \varepsilon) \tag{1}$$

To calculate the angle acceleration, Eq. (1) is differentiated twice, represented by Eq. (2):

$$\ddot{\theta} = -\theta_{\max}(\dot{\varphi})^2 \sin(\varphi + \varepsilon) \tag{2}$$

The pitch angle acceleration in Eq. (2) is maximized at 90 deg, and it is 8268 rad/s^2:

$$T = I_b \ddot{\theta} \tag{3}$$

Torque is 0.517 N · m through Eq. (3), and the control force becomes 17.2 N by dividing the torque by the distance from the pivot point to

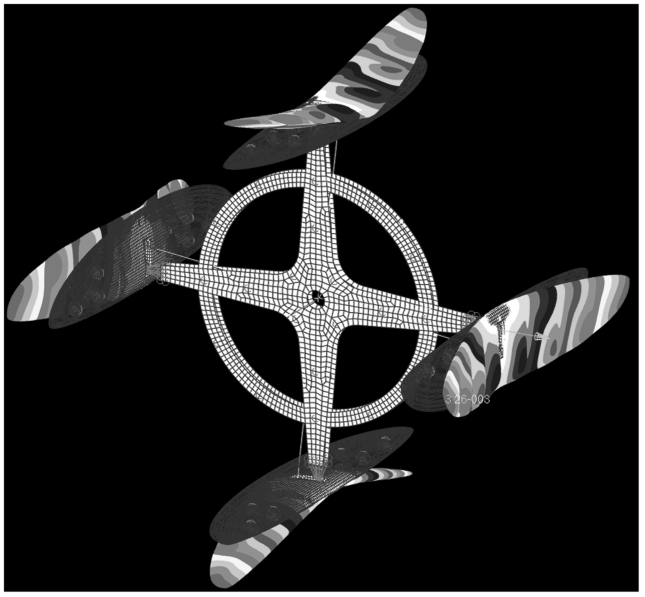

Fig. 11 Displacement distribution.

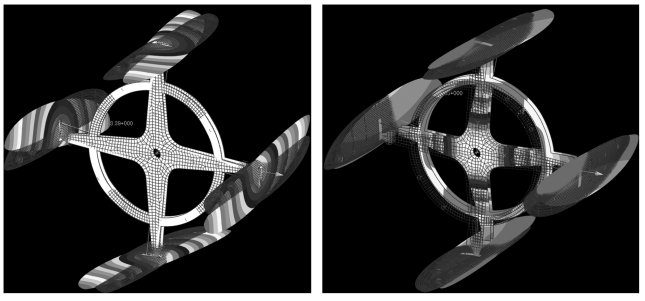

Fig. 12 Mode shape of the cyclocopter rotor (first and fourth modes).

the control point (30 mm). Therefore, the maximum control force by the blade inertia is 17.2 N. This value is not transmitted to the control servo because these forces counteract each other in the blades of opposite positions. This force is considered for the swash plate and control linkage design.

The effect of aerodynamic force was calculated. The cyclocopter rotor produces a thrust of 41.2 N. The force produced by one blade is maximized twice during one revolution when the pitch angle is maximized. Therefore, the maximum force on one blade is 20.6 N, and the transmitted force to the control linkage is 6.0 N when considering the distance between the aerodynamic center and pivot point. This force becomes 12.0 N per rotor, and it is delivered to the control servos. The control servo should be strong enough to withstand this force.

Figure 13 shows a diagram of the control mechanism and the calculation of the magnitude of the pitch angle change and the servo control force. When the blade pitch angle becomes 30 deg, the control center is moved 15 mm. At this condition, the servo horn is moved 9 mm, which equates to 34 deg. The control force is 19.9 N and the torque acting on the servo is 0.319 N · m. Table 3 shows the specification of the control servo that was selected for this control system. The output torque is sufficient to actuate the rotor blades.

Figure 14 shows the assembled control system using the swash plate and its realized picture. Pitch angles at azimuth angles 0 and 180 deg, and pitch angles at azimuth angles 90 and 270 deg, are operated independently at the developed control system. One servomotor powers the thrust of the back and forth direction, while the other one powers the up and down direction. Figure 15 shows two pitch angle variations; one curve represents when the pitch angle for the up/down direction is 20 deg and back/forth is 0 deg, and the other curve represents when the pitch angle for up/down is 20 deg and back/forth is 10 deg. As shown in Fig. 15, the pitch angles do not change at the azimuth angle 90 and 270 deg, which means there is independent actuation, although the maximum pitch angle becomes 22.4 deg.

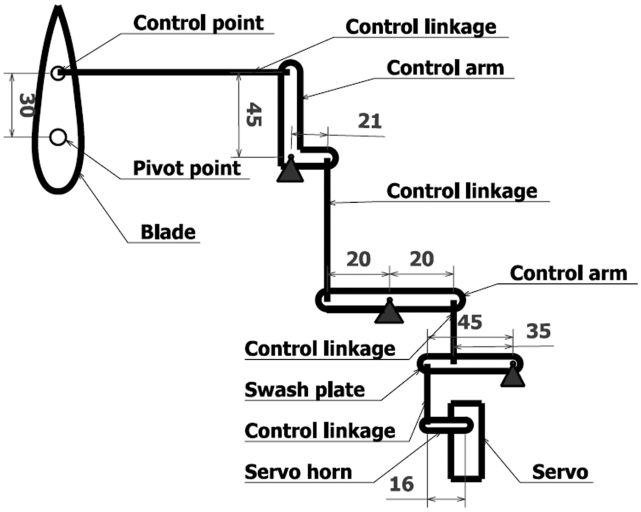

Fig. 13 Diagram of the control mechanism.

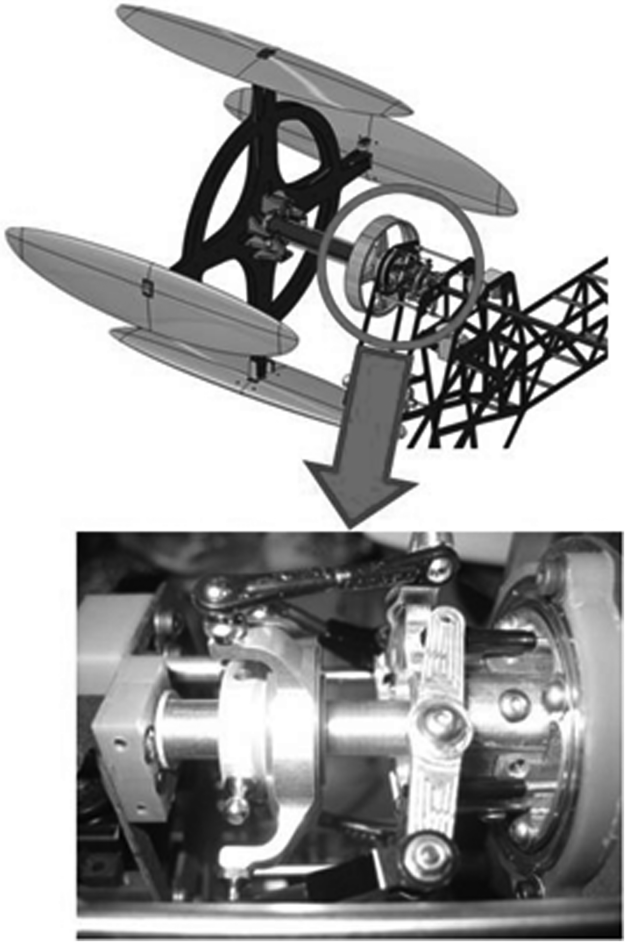

Fig. 14 Assembled control mechanism.

Table 3 HSR-5995TG servo specification

Operating speed	0.15 s/60 deg at 6.0 V
	0.12 s/60 deg at 7.4 V
Output torque	2.35 N · m at 6.0 V
	2.94 N · m at 7.4 V

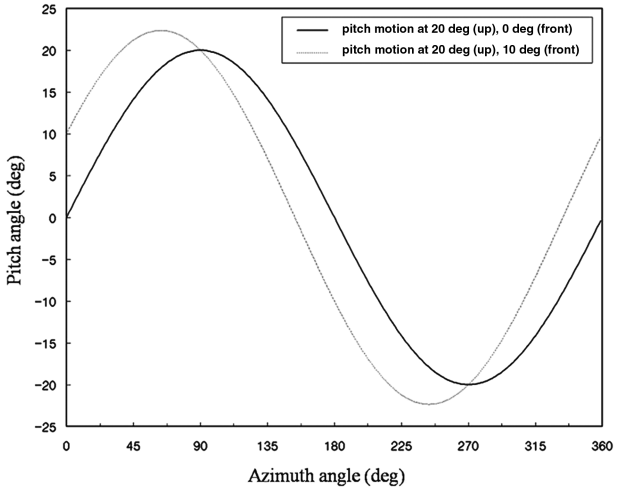

Fig. 15 Pitch angle variations.

IV. Design of the Power Transmission

The cyclocopter rotors are actuated by their own motors. This individual motor system has advantages in power transmission when compared with a one-motor system. Each rotor could be operated directly by its own motor, which means no additional large or complex driving transmissions are necessary. Four dc brushless type motors (Orbit 30-12 model) were installed, and lithium-polymer type batteries (PT-B2500N-PL model) were used. This battery consists of 3 unit cells of 3.7 V, and the maximum discharge rate is 22 C, 55 A. Two batteries connected in series supply 22.2 V to one rotor. When the motor speed is approximately 11,000 rpm, the reduction ratio of 9:1 is required for a rotor rotation of 1200 rpm. A timing-belt–pulley structure is applied for this reduction mechanism.

The rotating shaft connected with the belt–pulley device is a carbon composite pipe with a diameter of 25 mm, and another carbon composite pipe with a diameter of 10 mm is installed inside the large pipe. This inner pipe also has the role of supporting the swash plate. The cantilever type power transmission shaft should support a rotor of 1 kg with a thrust of 41.2 N, which is a relatively small amount. Therefore, static deflection does not cause a problem, but the shaft whirling could be a problem because of the weight at the tip of the shaft.

The critical speed of shaft whirling can be calculated by following equations, which are equations for the natural frequencies of a vibrating beam [19]:

$$f_c = \frac{1}{2\pi}\sqrt{\frac{3EI}{ML^3}} \tag{4}$$

$$f_d = 0.565\sqrt{\frac{gEI}{wL^4}} \tag{5}$$

where f_c is the frequency of the concentrated mass at the tip of the cantilever shaft, and f_d is the frequency of the distributed weight. The carbon composite shaft has a Young's modulus of 130 GPa. The area moment of inertia for the outer pipe (diameter 25 mm and thickness 1.0 mm) and the inner pipe (diameter 10 mm and thickness 1.3 mm) is 5.78e-9 m^4. The concentrated mass is 0.82 kg, including four blades, a hub arm, and control linkages, causing the variable M to become 49.2 N by adding a thrust of 41.2 N. The distributed weight of the rotating shaft itself is 1.83 N/m. The shaft length L is 0.19 m. Through these values, f_c is 40.73 Hz and f_d is 993.0 Hz, which results in the frequency of 40.69 Hz by Dunkerley's combination method. Therefore, the critical speed of shaft whirling is 2442 rpm, which is a higher speed than the designed rotating speed.

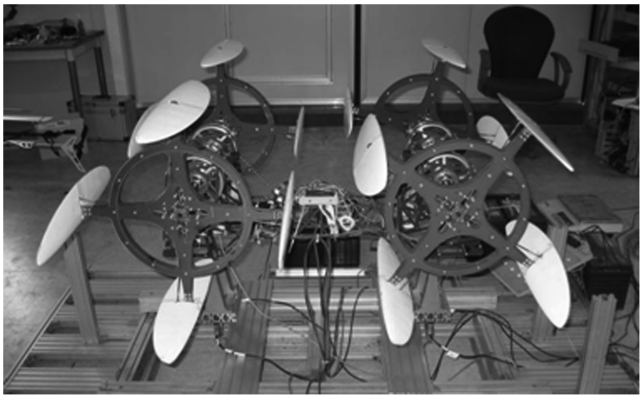

Fig. 16 Assembled cyclocopter.

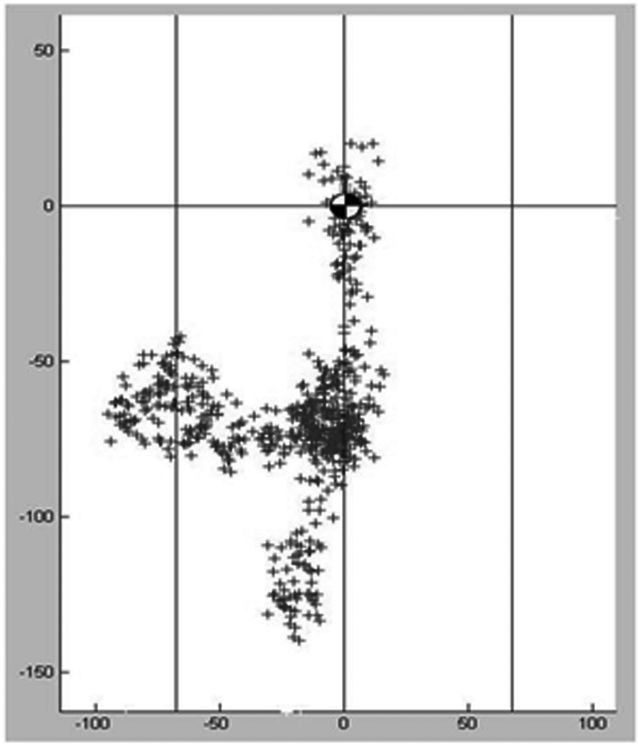

Fig. 17 Movement of the thrust center.

V. Experiment

The experiment was carried out to verify the performance of the designed cyclocopter. The thrust was measured by four load cells. The electric power consumption value and the rotating speed were measured by an electric device. Figure 16 shows the assembled cyclocopter on the test bed. As mentioned in the preceding section, the cyclocopter was designed to generate a thrust of 166 N by supplying 2240 W for the conditions of a maximum pitch angle of 25 deg and a rotating speed of 1130 rpm. The total weight of the cyclocopter including Li-Po batteries and landing gear was 12.0 kg.

The experimental results on the test bed gave a thrust of 157 N for the conditions of a maximum pitch angle of 25 deg and a rotating speed of 1100 rpm. The required power for this system was 2633 W. This experimental result is somewhat lower than the designed value, but the thrust is sufficient to maneuver a vertical takeoff, a landing, and a forward flight. The experimental power consumption value, which is approximately 15% higher than the designed value, could also be lower if the mechanical design is improved.

Figure 17 shows the movement of the thrust center of the cyclocopter. This result was obtained by measuring the thrust values of the four load cells. The thrust center in Fig. 17 is moving around

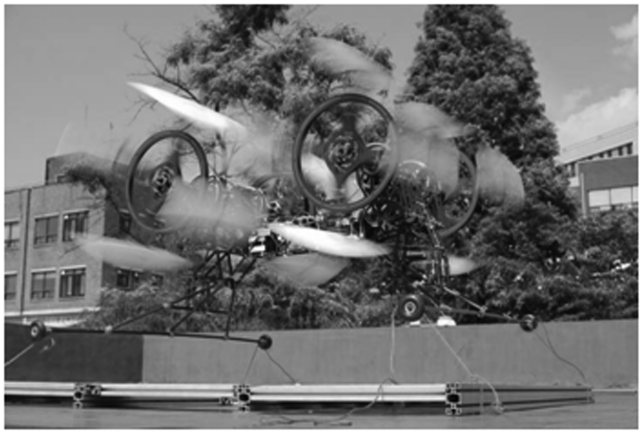

Fig. 18 Flight test of the cyclocopter.

the position of 70 mm behind the c.g. point. The movement in the left and right direction causes the rolling motion of the cyclocopter, whereas the up and down direction causes the pitching motion of cyclocopter. The attitude control of the cyclocopter could be accomplished from the information shown in this figure.

Figure 18 shows the flight test of the cyclocopter at a tethered condition. Although the aircraft attitude control is unstable, it achieved a breakthrough of success in hovering mode. We hope that we can show a more advanced flight test result through the configuration of this behavior after obtaining the appropriate maneuvering system.

VI. Conclusions

The present paper describes the design and development of the cyclocopter with four rotors. An elliptic blade was adopted, and rotor design parameters were determined through a CFD analysis. Static and dynamic structural analyses were carried out for the composite rotor blades system. For an efficient control system, a swash plate was applied to the cyclocopter rotor control mechanism. The control mechanism became compact and easy to control compared with the previous control system of the cyclocopter. Brushless dc motors and Li-Po batteries were used for operation of the rotor. Each rotor has its own control devices and power transmissions. The rotating shaft was constructed from carbon composite pipes. This shaft delivers power and supports the rotor blades. Shaft whirling was analyzed for the cantilevered beam structure. The measured thrust was sufficient to allow for a vertical takeoff and maneuvering. A flight test was also carried out under a tethered condition. Although attitude control of the cyclocopter was unstable, the experimental results showed that the cyclocopter could be an excellent VTOL aircraft. The experimental research to improve the performance of the cyclocopter is ongoing, and a flight test for a cyclocopter equipped with four rotors is in progress.

Acknowledgments

This research is partially supported by the second stage of the Brain Korea 21 Project in 2007 and the National Research Laboratory Program.

References

[1] Yun, C. Y., "A New Vertical Take-Off and Landing Aircraft with Cycloidal Blades System: Cyclocopter," Ph.D. Dissertation, Seoul National Univ., Seoul, Korea, 2004.

[2] Wheatley, J. B., "Simplified Aerodynamic Analysis of the Cyclogiro Rotating-Wing System," NACA Technical Notes No. 467, Aug. 1933.

[3] Wheatley, J. B., and Windler, R., "Wind-Tunnel Tests of a Cyclogiro Rotor," NACA Technical Notes No. 528, May 1935.

[4] Kirsten, F. K., "Cycloidal Propulsion Applied to Aircraft," *Transactions of the American Society of Mechanical Engineers*, Vol. 50, No. AER–50–12, 1928, pp. 25–48.

[5] Kirsten, F. K., "Cycloidal Propulsion in Air," *Engineering Experiment Station Series Bulletin No. 79*, Univ. of Washington, Seattle, WA, March 1935.

[6] Eastman, F. S., Burkheimer, G., and Cotter, W. E., "Wind Tunnel Tests on a High Pitch Cyclogiro," Univ. of Washington Aeronautical Lab. Rept. No. 191-A, Univ. of Washington, Seattle, WA, June 1943.

[7] Eastman, F. S., "The Full-Feathering Cyclogiro," Univ. of Washington Aeronautical Lab. Rept. No. 317, Univ. of Washington, Seattle, WA, March 1951.

[8] Gibbens, R. P., and Boschma, J. H., "Construction and Testing of a New Aircraft Cycloidal Propeller," *13th AIAA Lighter-Than-Air Systems Technology Conference*, AIAA 99-3906, 1999.

[9] Boschma, J. H., "Modern Aviation Applications for Cycloidal Propulsion," *AIAA Aircraft, Technology Integration, and Operations Forum*, AIAA 2001-5267, Oct. 2001.

[10] Sirohi, J., Parsons, E., and Chopra, I., "Hover Performance of a Cycloidal Rotor for a Micro Air Vehicle," *Journal of the American Helicopter Society*, Vol. 52, No. 3, 2007, pp. 263–279.

[11] Iosilevskii, G., and Levy, Y., "Experimental and Numerical Study of Cyclogiro Aerodynamics," *AIAA Journal*, Vol. 44, No. 12, 2006, pp. 2866–2870.
doi:10.2514/1.8227

[12] Hu, Y., Lim, K. B., and Hu, W. R., "Research on the Performance of Cyclogiro," *6th AIAA Aviation Technology, Integration and Operations Conference*, AIAA 2006-7704, Sept. 2006.

[13] Higashi, Y., Tanaka, K., Emaru, T., and Wang, H. O., "Development of a Cyclogyro-Based Flying Robot with Variable Attack Angle Mechanisms," *IEEE/ASME Transactons on Mechatronics*, Vol. 12, No. 5, 2007, pp. 565–570.

[14] Anderson, J. D., *Fundamentals of Aerodynamics*, 2nd ed., McGraw–Hill, New York, 1991, pp. 315–375.

[15] Hwang, I. S., Min, S. Y., Kim, M. K., and Kim, S. J., "Multidisciplinary Optimal Design of Cyclocopter Blade System," *1st AIAA Multi-Disciplinary Optimization Specialist Conference*, AIAA 2005-2287, April 2005.

[16] MSC.PATRAN PCL Reference Guide, MSC Software, Santa Ana, CA, 2003.

[17] STAR-CD Ver. 3.20 User Guide, CD-Adapco Group, New York, 2004.

[18] MSC.NASTRAN User's Manual, MSC Software, Santa Ana, CA, 2003.

[19] Meirovitch, L., *Elements of Vibration Analysis*, 2nd ed., McGraw–Hill, New York, 1986, pp. 58–63.